HHS Public Access

Author manuscript

J Phys Chem B. Author manuscript; available in PMC 2024 June 27.

Published in final edited form as:

J Phys Chem B. 2023 March 23; 127(11): 2289–2301. doi:10.1021/acs.jpcb.2c07330.

Singlet Molecular Oxygen: from COIL Lasers to Photodynamic Cancer Therapy

S. J. Davis,
Physical Sciences Inc., 20 New England Business Center, Andover, Massachusetts 01810, United States

Y. Zhao,
Physical Sciences Inc., 20 New England Business Center, Andover, Massachusetts 01810, United States

T. C. Yu,
Physical Sciences Inc., 20 New England Business Center, Andover, Massachusetts 01810, United States

E. V. Maytin,
Departments of Biomedical Engineering and Dermatology, Cleveland Clinic, Cleveland, Ohio 44195, United States

S. Anand,
Departments of Biomedical Engineering and Dermatology, Cleveland Clinic, Cleveland, Ohio 44195, United States

T. Hasan,
Wellman Center for Photomedicine, Boston, Massachusetts 02114, United States

B. W. Pogue
Department of Medical Physics, Wisconsin Institutes for Medical Research, Madison, Wisconsin 53705, United States

Abstract

Translation of experimental techniques from one scientific discipline to another is often difficult but rewarding. Knowledge gained from the new area can lead to long lasting and fruitful collaborations with concomitant development of new ideas and studies. In this Review Article, we describe how early work on the chemically pumped atomic iodine laser (COIL) led to the development of a key diagnostic for a promising cancer treatment known as photodynamic therapy (PDT). The highly metastable excited state of molecular oxygen, $a^1\Delta_g$, also known as singlet oxygen, is the link between these disparate fields. It powers the COIL laser and is the active species that kills cancer cells during PDT. We describe the fundamentals of both COIL and PDT and trace the development path of an ultrasensitive dosimeter for singlet oxygen. The path from

Corresponding Author: S. J. Davis – *Physical Sciences Inc., 20 New England Business Center, Andover, Massachusetts 01810, United States;* davis@psicorp.com.

The authors declare no competing financial interest.

Complete contact information is available at: https://pubs.acs.org/10.1021/acs.jpcb.2c07330

COIL lasers to cancer research was relatively long and required medical and engineering expertise from numerous collaborations. As we show below, the knowledge gained in the COIL research, combined with these extensive collaborations, has resulted in our being able to show a strong correlation between cancer cell death and the singlet oxygen measured during PDT treatments of mice. This progress is a key step in the eventual development of a singlet oxygen dosimeter that could be used to guide PDT treatments and improve outcomes.

Graphical Abstract

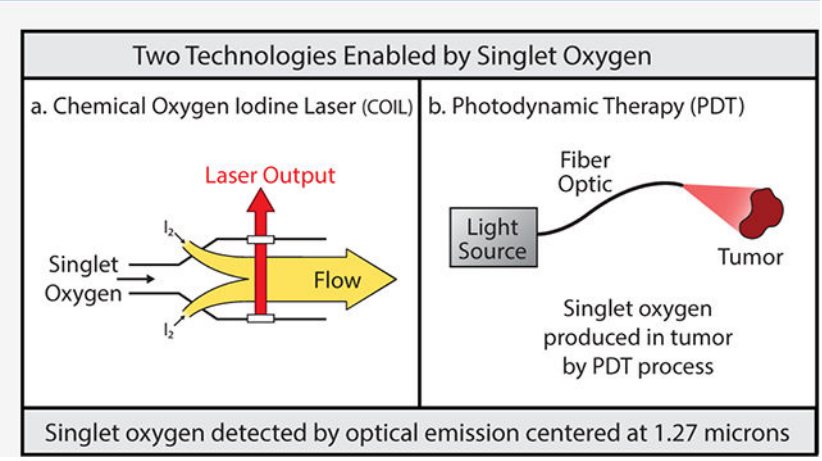

INTRODUCTION

In this paper, we describe the unanticipated journey from basic research in chemical lasers to a promising cancer treatment known as Photodynamic Therapy (PDT). The common thread between these two disparate areas is the lowest electronically excited state of molecular oxygen, $a^1\Delta_g$. As we discuss below, this state, which we will call singlet oxygen, is the power source for the chemical oxygen iodine laser (COIL) and also the species responsible for selective destruction of cancer cells in PDT. In order to describe the connections between these two widely different applications of singlet oxygen, we present a short summary of the history of COIL and a description of PDT. These two developments cover a period of over four decades.

To assist the reader, we have organized the paper as follows: In the first third of the paper, we describe chemical lasers in general and then focus on COIL and how we developed early singlet oxygen diagnostics. The remainder of the paper covers the subsequent transition to PDT from first attempts with *in vitro* liquid samples through our current *in vivo* studies on living mice. We hope that these organizational comments assist the reader in following our path from one discipline to another very different one.

Background of Chemical Lasers.

Beginning in the early 1970s, there was considerable national interest in developing gas-phase chemical lasers. These devices use chemical reactions to produce population inversions between the lasing species energy levels. A classic example is the hydrogen

fluoride (HF) chemical laser. Fluorine atoms react with molecular hydrogen to produce directly, vibrationally excited HF(v) with population inversions among several vibrational–rotational (v, J) levels as described by reaction 1:

$$F + H_2 \rightarrow HF(v, J) + H \quad (1)$$

An analogous reaction between fluorine atoms and deuterium produces deuterium fluoride with population inversions. High power lasers for HF and DF were developed in supersonic flowing gas systems. Both HF and DF produce numerous wavelengths with averages of 2.7 and 3.6 μm, respectively. Continuous wave (cw) laser outputs of these devices have exceeded 100 kW.

However, due to diffraction, the relatively long wavelengths of these devices limited the spot size that could be focused onto a target. In addition, the HF laser had poor propagation in the atmosphere due to water vapor absorption. Thus, there was considerable interest in identifying and developing a shorter wavelength chemical laser that also had good atmospheric propagation. This led to a search for shorter wavelength systems that could use smaller, lighter, optical trains. One potential system was the atomic iodine laser that operates at 1.315 μm. Kasper and Pimentel reported the first observations of lasing in 1964.[1] They used a pulsed flashlamp to selectively photodissociate alkyl-iodide molecules to the atomic iodine $^2P_{1/2}$ state, the upper laser level.

Basics of the Chemical Oxygen Iodine Laser.

In a seminal series of low pressure discharge flow tube chemiluminescence studies, Derwent and Thrush[2–6] at Cambridge University concluded that the atomic iodine $5^2P_{1/2} \rightarrow 5^2P_{3/2}$ transition would be an excellent candidate system for energy transfer pumping from the highly metastable singlet molecular oxygen molecule, $O_2(a^1\Delta_g)$. Indeed, they predicted that an atomic iodine laser could be produced if the molecular oxygen flow contained at least 18% $O_2(a^1\Delta_g)$. The energy levels of molecular oxygen and the iodine atom are shown in Figure 1. Note that the iodine atom has hyperfine structure. The laser operates on the $F' = 3$ to $F'' = 4$ transition.

The $a^1\Delta_g$ lies 7882 cm^{-1} above the ground $X^3\sum_g$ state; thus, it has sufficient energy to collisionally pump the iodine atom to the excited $5^2P_{1/2}$ state.

In late 1977, McDermott et al.[7] demonstrated the first chemical oxygen iodine laser (COIL) using this energy transfer scheme and state selective chemistry to produce singlet oxygen. They used a gas/liquid phase sparger generator to produce the singlet oxygen by bubbling chlorine gas through a solution of H_2O_2 buffered with NaOH. The chlorine gas diffused into the liquid and reacted rapidly with the HO_2^- ion to produce greater than 25% singlet oxygen vs ground state $O_2(X^3\sum)$. Subsequent research has shown that the inherent yield of the chlorine/buffered H_2O_2 is essentially 100% $O_2(^1\Delta_g)$.[8] Since the diffusion process is slow,

this reaction occurs near the gas–liquid boundary, allowing the $O_2(^1\Delta_g)$ to diffuse back into the gas phase. The overall stoichiometry of the singlet O_2 generation is shown in reaction 2:

$$Cl_2 + 2MOH + H_2O_2 \rightarrow O_2(a^1\Delta) + 2MCl + 2H_2O \quad (2)$$

where M is an alkali metal ion.

At high $O_2(^1\Delta_g)$ concentrations in the gas phase, the dominant loss is through the energy pooling process, illustrated by reaction 3.

$$O_2(a^1\Delta_g) + O_2(a^1\Delta_g) \rightarrow O_2(b^1\Sigma_u) + O_2(X^3\Sigma) \quad (3)$$

Thus, flow from the gas–liquid generator to the laser nozzle must be rapid. Indeed, COIL devices, similar to chemically pumped HF and DF systems, are flowing gas systems, typically supersonic. The flows provide excess heat removal to ensure that the laser region of the flow always has a fresh laser medium in the active volume of the optical resonator. In all COIL devices, the chemical generator for singlet O_2 is upstream of the nozzle where molecular iodine in mixed into the singlet O_2 flow. Through a not thoroughly understood mechanism,[9–13] the singlet oxygen flow dissociates the $5^2P_{1/2}$, and the I atoms are rapidly pumped to the $5^2P_{1/2}$ state. A strong equilibrium is established in this region of the flow, as described by reaction 4.

$$O_2(a) + I \underset{k_r}{\overset{k_f}{\rightleftharpoons}} O_2(X) + I^* + \Delta E \quad \Delta E = 279\text{cm}^{-1} \quad (4)$$

where k_f and k_r are the rate coefficients for the pumping and reverse reaction, respectively.

In COIL, the optical gain is produced by the atomic iodine, and as lasing commences, the extracted power is produced by the singlet oxygen through the pumping reaction. Therefore, accurate, nonintrusive diagnostics for singlet O_2 were essential for developing accurate models to scale the output power.

The McDermott et al. paper rapidly generated intense interest in the COIL device, and in the intervening years, there have been hundreds of papers published worldwide describing both fundamental kinetics and engineering kinetics of the COIL device. We would also like to mention the pioneering work of Carroll et al.[14–17] who demonstrated an electrical variant of COIL by using a radio frequency discharge to produce the singlet O_2, eliminating the need

for a chemical generator. Similar results by Rawlins and co-workers[18] were later achieved using a microwave discharge to produce the singlet O_2. COIL was eventually scaled to a MW-class laser. These developments will not be discussed here, but summaries of COIL, HF, and DF lasers are contained in refs 19 and 20.

One of the authors of this current paper, S.J.D., was an early investigator of the COIL device and began developing optical diagnostics to probe for key species in the reacting flowfield which included both the excited iodine atom and singlet oxygen. In the gas phase, the $O_2(a^1\Delta_g)$ state has a very long radiative lifetime, approximately 72 min. Consequently, the emission, centered at ~ 1.27 μm, is exceedingly weak. In the early phase of COIL (late 1970s), there were only two optical detectors capable of detecting this short wavelength infrared (SWIR) radiation: a dry ice-cooled photomultiplier tube (PMT) or a liquid nitrogen cooled intrinsic Ge detector (Applied Detector Technologies). The PMTs at that time had a quantum efficiency of only ~0.001%. In contrast, the Ge photodiode detector had high quantum efficiency (>50%) and excellent sensitivity (D^* ~10^{15} cm^2 $Hz^{1/2}$/W) but required liquid-nitrogen-cooled transimpedance amplifiers to amplify the weak signals, and the amplifiers operated at what is known as the “gain/bandwidth limit”. This limited the highest sensitivity Ge devices to a temporal response time of ~1 ms. While this precluded some time-resolved studies, the Ge detector proved a valuable tool for steady state investigations of singlet oxygen and iodine atoms in the reacting gaseous flows. The Ge detector was sensitive enough to be coupled with standard 0.3 m monochromators to spectroscopically resolve the gross features of the singlet oxygen spectrum. Because the radiative lifetime of the $O_2(^1\Delta_g)$ state is known, one can measure its concentration using a blackbody calibrated spectrometer/detector system. The germanium detectors were used by many laboratories involved with COIL research to help understand the basic physics and to anchor models scaling COIL to high output powers. Indeed, as COIL was scaled to higher powers, the germanium detector-based singlet oxygen monitor was a key diagnostic. Eventually, with the advancement of commercially available, much more sensitive SWIR detection systems such as the Princeton Instruments liquid nitrogen cooled InGaAs Optical Multichannel Analyzer, it became possible to spectrally resolve the rotational structure of the singlet oxygen emission in gas flows. Figure 2 shows a spectrum of rotationally resolved singlet oxygen emission produced by a low pressure 2450 MHz discharge of an Ar/O_2 flow. The observed spectrum is shown in black, and a spectral fit to the data is shown in red. Spectral fitting significantly increases the precision of determining the area under the spectrum. This area is directly proportional to the population density of the emitting $O_2(^1\Delta_g)$ state.

Next, we discuss how the lessons learned in developing singlet oxygen detection for COIL have been successfully applied to develop a singlet oxygen dosimeter for photodynamic therapy.

Fundamentals of Photodynamic Therapy.

Within the same time period as research described above, numerous researchers were exploring possible medical applications of lasers. These included relatively low power commercially available devices such as tunable dye lasers and solid state lasers. The

potential for cancer treatment using lasers generated considerable interest, and PDT emerged as a very promising area. PDT is a photoinduced process with the earliest reports dating back to 1900 in experiments by Raab Ueber.[21] Three essential ingredients are required for this process: (1) a photosensitizer (PS) molecule, (2) a light source, and (3) oxygen. The PS molecules absorb the photons from the light source and subsequently collisionally excite the singlet O_2 state. Kautsky and de Bruijn[22] published initial definitive studies in 1931. In 1976, Weishaupt et al. reported convincing evidence that singlet oxygen was the species responsible for killing tumors.[23] In a set of experiments, they used filtered light at 630 nm to irradiate tumor samples in aqueous oxygenated solutions of hematoporphyrin derivative (HPD) photosensitizer. They showed that cancer cells suspended in a PS solution and exposed to the excitation light were killed. When they added an efficient quencher of singlet oxygen to the PS solution and repeated the experiments, the cancer cells survived, strongly implying that singlet oxygen was the cytotoxic agent. Subsequent studies have shown that PDT excited state singlet O_2 is responsible for the cell destruction by (a) direct damage to cell walls and mitochondria[24] and (b) vascular constriction that deprives the tumor of nutrients.[25]

Singlet O_2 and Its Role in PDT.

FDA approval has been granted for PDT treatment of esophageal adenocarcinoma, high-grade dysplasia, and certain lung cancers. PDT is also being applied to important areas outside of cancer treatment, including age related macular degeneration and actinic keratosis, a precancerous skin condition. In PDT, the singlet O_2 is produced via the mechanism shown in Figure 3.

PDT treatment depends upon several parameters: (a) the PS concentration in the tumor, (b) tumor oxygenation, and (c) total light dose (fluence). The PDT dose is defined as $\int [\mathrm{PS}(t)] \times [\mathrm{O}_2] \ \Phi(t) \mathrm{d}t$. Currently, there are no *in vivo* capable singlet O_2 dosimeters used during PDT treatment, so these key parameters of PDT treatment are unquantifiable to physicians in the clinic. Evidence increasingly indicates that treatment outcome and variation have a strong correlation with the amount of singlet O_2 produced within the tumor.[24–38] Thus, accurate singlet O_2 dosimetry would have a significant impact on the advancement of PDT in cancer treatment.

METHOD AND RESULTS

Note that since we discuss the evolution of our singlet oxygen dosimeter development for PDT through several stages, we present both Methods and Results for each subsection below.

In Vitro Studies.

The weak optical emission from singlet oxygen presents a significant challenge for developing an optically based monitor, especially for *in vivo* applications. It is a much more challenging medium than the reactive gas flow in COIL. First, the PS, when irradiated with a light source (400 to 700 nm depending on the particular PS), radiates back to its ground state via an allowed transition (radiative lifetime ~ 10 ns). Since the potential curves of most

photosensitizers' excited singlet states are slightly displaced relative to that of the ground state, the radiative emission has an extended, longer wavelength red tail that extends beyond the singlet O_2 center at 1.27 μm. This presents a strong spectral background interference. In addition, singlet O_2 is severely quenched in tissue (quenching lifetime of 4 μs in aqueous media and as short as 0.1 μs in biological media[35–40]). In contrast to rotationally resolved emission from singlet O_2 in gaseous media, the spectrum is broadened into relatively narrow continuum (fwhm of ~ 20 nm) centered at ~1.27 μm in liquid environments. Thus, no rotational structure exists to leverage a more accurate determination of the total singlet oxygen emission through spectral fitting techniques.

Next, we discuss how we used combinations of spectral and temporal filtering to discriminate the singlet oxygen luminescence emission from the PS fluorescence.

In our initial investigations, we took advantage of temporal discrimination to enhance the signal-to-noise ratio of the singlet O_2. We used a diode laser modulated by a square wave current generator to produce a continuous train of square wave output pulses to excite the PS. As shown in Figure 4, while the laser is on, the PS is being excited and simultaneously emits throughout the visible to the short wavelength infrared spectral region that includes the singlet oxygen luminescence spectral region. This PS fluorescence in the singlet oxygen luminescence spectral region 1.2 to 1.3 μm is several orders of magnitude weaker than at the PS light source excitation wavelength. Nevertheless, it presents a strong interference background. Between pulses, when the diode laser is off, the PS fluorescence rapidly decays and the longer-lived and weaker singlet O_2 luminescence can be observed in this "dark" time interval. In our initial studies, we used a novel Hamamatsu photomultiplier tube (PMT) with a time response <10 ns and photon counting capabilities.

The overall experimental setup for these initial studies is illustrated in Figure 5. The system consisted of four major elements: (a) a fiber coupled, pulsed diode laser; (b) a liquid light guide (LLG) to collect the SWIR emission from PS and singlet oxygen; (c) a photon counting PMT; and (d) a data acquisition and analysis system.

We used a fiber coupled diode laser with an output wavelength of 655 nm. In the pulsed mode, this device typically produced less than 1 μJ/pulse. Pulse lengths of 1, 2, and 5 μs were used in these studies. A Hamamatsu (5509–42) photomultiplier tube (PMT) was used for detection of the singlet oxygen emission. The fiber optic output illuminated a 1 cm diameter spot on the side of the cuvette, and the near-IR emission was collected with a 1.5-mm-diameter light guide that transmitted greater than 80% at 1.27 μm. The output beam of the LLG was collimated and sent through a pair of RG 1000 filters and a narrow bandpass filter centered at 1.27 μm and was directed into the input of the photomultiplier tube. The PMT had a quantum efficiency of about 1% at the singlet oxygen emission wavelength and a temporal response of less than 10 ns. Three solvents were used to provide a variety of quenching environments: acetone, methanol, and water. Since the lifetimes of singlet oxygen are known in these solvents,[35–40] they provided an excellent test of our system. Photosensitizers were procured from Frontier Scientific and solvents from Fisher Scientific. PS concentrations ranged from 10^{-3} M to 10^{-6} M and were prepared. All prepared PS

solutions were kept in amber glass bottles to minimize photobleaching from ambient light. The PS studied are summarized in Table 1.

We completed a matrix of runs using the photosensitizers listed above and excitation pulse lengths of 1, 2, and 5 μs. Pulse repetition rates of 500 and 1000 Hz were used. In the following figures, we present some of the extensive data generated.

Figure 6 shows data for Cl-e6 in acetone (6a) and water (6b) for a 5 μs excitation pulse width. For these examples, while the square wave diode laser pulse is on, the signal strength of the PS fluorescence is 100 (arbitrary units) on both plots. The production of singlet O_2 (via transfer from the photosensitizer triplet state) and its subsequent quenching (by the solvent molecules) are evident. Indeed, for the acetone solvent case (relatively weak quenching), the observed signal from singlet oxygen is several times greater than that from the photosensitizer. Note, as well, the dramatic reduction in τ_Δ due to water quenching when compared to acetone.

Figure 7 compares the observed temporal profiles for Cl-e6 in water for two diode laser pulse widths: 2 and 5 μs. The increasing signal while the laser is on is due to a rising singlet oxygen concentration. Indeed, inspection of the data in Figure 7 shows that the singlet oxygen concentration during the diode laser pulse has not reached a maximum value even after 5 μs.

In order to support interpretation of the experimental data, we developed a model for the singlet O_2 production and emission kinetics relevant to our long pulse (1–10 μs) diode laser pulsed excitation. From Figure 3, we developed rate equations to describe the temporal evolutions of the relevant species concentrations: $[S_o]$, the ground singlet state of the PS; $[S_1]$, the excited singlet state of the PS; $[T_1]$, the excited triplet state of the PS; and $\left[O_2\left(^1\Delta\right)\right]$, the singlet state of O_2. The relevant equations are

$$\frac{d[S_1]}{dt} = I\sigma[S_o] - [S_1]/\tau_{S_1} \tag{5}$$

$$\frac{d[T_1]}{dt} = [S_1]K_{S_1 \to T_1} - [T_1]/\tau_{T_1} \tag{6}$$

$$\frac{d[O_2(^1\Delta)]}{dt} = [T_1]K_{T_1 \to {}^1\Delta} - \left[O_2{}^1\Delta\right]/\tau_\Delta \tag{7}$$

where I is the excitation laser intensity in photons cm^{-2} s^{-1}, σ is the absorption cross section of the photosensitizer, $1/\tau_{S_1}$ is the total removal rate from S_1, $K_{S_1 \to T_1}$ is the intrasystem

transfer rate from $S_1 \rightarrow T_1$, $1/\tau_{T1}$ is the total removal rate from T_1, $K_{T_1} \rightarrow {}^1\Delta$ is the collisional transfer rate from state T_1 of the photosensitizer to the ${}^1\Delta$ state of oxygen, $1/\tau_{T_\Delta}$ is the total removal rate from the ${}^1\Delta$ state of oxygen, and $\left[O_2\left({}^1\Delta\right)\right]$ is the singlet oxygen concentration in cm^{-3} as a function of time (t).

Treating the excitation pulse as an "instantaneous" source, such as a Q-switched, frequency doubled Nd:YAG laser, leads to a time dependent solution for the singlet O_2 concentration after the termination of the excitation pulse:

$$\left[O_2\left({}^1\Delta\right)\right]_t = N\sigma[S_o]\Phi_\Delta \frac{\tau_\Delta}{\tau_T - \tau_\Delta}\left\{e^{-t/\tau_T} - e^{-t/\tau_\Delta}\right\} \quad (8)$$

where N is the total photon fluence delivered to the Φ_Δ is the yield of $O_2\left({}^1\Delta\right)$ from absorption of a pump photon by the PS. Our diode laser-based system uses much longer pulse widths, between 1 and 10 μs, so the instantaneous excitation constant over the duration of the laser pulse. To gain a better model is no longer valid. In our case, the diode laser intensity is constant over the duration of the laser pulse. To gain a better understanding of this limit, we solved eqs 5 through 7 numerically. In Figure 8, we show the temporal evolutions of all three important states in the type II PDT process: singlet and triplet states of the PS and the singlet molecular O_2. As shown in Figure 8, during the diode laser pulse, the population of the PS singlet state quickly reaches a steady state value. The PS triplet state population grows and collisionally populates the O_2 singlet state. When the diode laser turns off, an equation of the form of eq 7 still applies.

We used this model and fitted the data to determine kinetic rates and lifetimes for both the PS triplet state and the singlet oxygen state. Our measured values are shown in Table 2.

Figure 9a and b show comparisons of this model to our data. It is important to note that for many photosensitizers there is some prompt, singlet state emission at the singlet O_2 emission wavelength (~1.27 μm). However, this emission decays in a few nanoseconds after the diode laser pulse is terminated. This is predicted by our model and clearly observed in our experiment as shown in Figure 9. The singlet O_2 production also occurs while the diode laser is on. The model accurately predicts singlet O_2 production in the solution phase with PDT treatment parameters such as PS concentration, laser intensity, PS triplet lifetime, singlet O_2 lifetime, and transfer rates.

We note that Wilson et al.[33,36–38] have used a similar PMT with both a frequency doubled Nd:YAG laser (10 ns pulses) and a pulsed optical parametric oscillator (OPO). Since their laser pulsewidths were so short (~10 ns), they could use the instantaneous model of eq 8 above.

To verify that the observed signals were indeed from singlet oxygen, we included the capability for oxygenating and deoxygenating the liquid samples in the cuvettes. A small Teflon cap that contained a pair of stainless steel tubes to introduce N_2 into the samples was

attached to the cuvette as shown in Figure 10. To deoxygenate the solution, nitrogen gas was slowly bubbled through the cuvette. Figure 11 shows a comparison of data from a Cl-e6 sample in water both oxygenated and deoxygenated. The diode laser pulse width was 2 μs for this data. Nitrogen is bubbled in to displace the dissolved oxygen. This removed both the rising part of the emission during the diode laser pulse and the emission after the termination of the diode laser pulse. These data provide unambiguous proof that the observed signals do indeed arise from singlet oxygen. The emission remaining in oxygen-depleted solvent is due to weak IR emission (at 1.27 μm) from the photosensitizer singlet state. It reproduces the diode laser emission pulse and is consistent with our model described above and illustrated in Figure 8.

When the N_2 flow was shut off, ambient oxygen diffused back into the cuvette and the singlet oxygen signal shown in Figure 11a returned.

Temporal and Spectral Discrimination Methods.

These initial experiments convinced us that our pulsed diode laser approach could detect singlet O_2 emission *in vitro* in highly quenching media. However, for *in vivo* measurements in this wavelength region, there are also other possible emission sources besides the singlet O_2 emission, such as broadband PS fluorescence and phosphorescence, optical component emission, and tissue autofluorescence. Thus, we added a simple spectral discrimination method to detect very weak emission signal from singlet oxygen at concentration levels as low as a few hundred picomolar. We used a set of three narrow bandpass ($\Delta\lambda$=15 nm) optical filters (1.22, 1.27, and 1.32 μm) and a slider that held the three filters to sequentially detect the singlet O_2 emission signal and background signals. The emissions at 1.22 and 1.32 μm contain only PS fluorescence, and the emission at 1.27 μm contains contributions from both the singlet O_2 and PS. Figure 12 shows a conceptual diagram of the typical PS emission and the transmission curves with the three filters. By recording all three wavelengths in each PDT experiment, we were able to subtract off most of the PS emission baseline from the recorded signal. The capabilities of this approach are demonstrated in animal studies as discussed below.

In Vivo Experiments in a Rat Prostate Cancer Model.

Our first *in vivo* study was performed at the Massachusetts General Hospital. This animal model uses the R3327-MatLyLu prostate cancer cell line that follows the human disease pattern and metastasizes into lymph nodes and lungs. Since the R3327-MatLyLu cells are syngeneic, there is no need for immune suppression in the rats, which enhances the model's clinical relevance. This study was performed under MGH protocol #2004N000270/1.

Tumor Induction.—Tumors were induced by subcutaneous injection of a suspension of 10^5 R3327-MatLyLu cells into the flanks of two-months-old male Copenhagen rats of 150 to 200 g weight. Implant sizes were repeatedly assessed by caliper measurement. Tumor volumes (V) were calculated using the equation for an ellipsoid: $V = \text{length} \times \text{width} \times \text{height} \times \pi/6$. Tumors were observed while growing to treatment dimensions of about 0.3 cm^3, which requires approximately 8 to 10 days.

Photosensitization.—Once the tumors had reached treatment size, the animals received an injection of photosensitizer, either intravenous Cl-e6, BPD, or intraperitoneal amino-levulinic acid (ALA). After waiting 3 h to allow for photosensitizer (PS) accumulation in the tumor, light exposure was done in the anesthetized animals through shaved skin. Irradiations of the tumors were performed using a commercial, continuous wave diode laser source (HPD, Inc.) designed for PDT with an output wavelength that matched the absorption profile of the PS.

Singlet Oxygen Measurements.—Before the therapeutic light exposure with the cw treatment laser, the singlet oxygen liquid light guide probe was set up to allow for tumor surface observation. The singlet oxygen luminescence was recorded immediately before starting the therapeutic light exposure, at several separate times during the irradiation, and at the end of the light exposure. Each measurement consisted of approximately 30 000 pulses with the pulsed diode laser source, and the signal photoelectrons were summed. The measurement required interrupting the therapeutic light exposure, but only for approximately 10 to 30 s.

Tumor Regression Measurements.—Following the PDT treatment with different photosensitizer dosages and light dosages, the tumor size was measured each day for 14 days. In Figures 13 and 14, we present some results of tumor growth and regression following the treatment. Figure 13 illustrates the tumor regression measured for three rats as a function of the singlet oxygen measured during the PDT treatment. One was a control with no PS injection or light dosage. One rat produced a relatively small singlet oxygen signal and showed steady tumor growth similar to the control. The rat (red diamonds) that produced the most singlet oxygen (approximately 6 times that of the one indicated with blue squares) showed a tumor regression of ~90% 2 days after the treatment. Tumor growth then began again. (The PDT dosages were not intended to be curative). In Figure 14, we plot the tumor regression 2 days after treatment produced in a cohort of 7 rats as a function of the singlet oxygen measured during the PDT treatment. The error bars represent expected uncertainties in measuring tumor size and the standard deviation of the number of singlet oxygen photoelectrons detected. The data indicate larger systematic uncertainties that pertain to variations in singlet oxygen production and treatment outcome for different animals.

While these are preliminary data from a limited number of animals, there does appear to be a clear correlation between the reduction of the tumor mass regression and the amount of singlet oxygen produced (photoelectron counts). These represented the first data of this kind from *in vivo* studies.[33] More recently, we performed similar experiments at Dart-mouth College using a short wave infrared camera to obtain simultaneous images of both singlet O_2 and PS from tumors implanted on mice.[41]

CW Singlet Oxygen Monitoring.

The studies using a pulsed diode laser, as presented above, demonstrated singlet oxygen detection *in vivo* by extracting the longer-lived singlet O_2 signal from prompt PS fluorescence. Others have also evaluated the time-gated approach for singlet O_2 detection

and demonstrated its value in PDT studies.[36–38,42,43] As discussed earlier, this approach allowed us to observe the singlet oxygen in dark time after the termination of the diode laser pulse. While that essentially eliminated the background PS fluorescence and increased the signal-to-noise ratio for the singlet oxygen, it was not optimal as a singlet oxygen monitor for potential clinical use. First, it required a dedicated diode laser, separate from a treatment laser, to produce the singlet oxygen we measured. In a typical PDT treatment, the cw treatment laser is on for several minutes. In our studies described above the treatment laser was shut off for 30 s intervals several times during the treatment so that we could make our measurements. This clearly would not be compatible with existing PDT protocols. In addition, our pulsed diode laser technique did not measure the singlet O_2 produced while the cw treatment laser was on. Rather, it measured the capability of the tumor that contains the PS and oxygen to produce singlet O_2. Consequently, we most recently have further developed our approach to observe singlet O_2 produced directly from a cw clinical PDT treatment laser.

For these cw measurements, the relatively narrow singlet oxygen luminescence centered at 1.27 μm must be spectrally discriminated from the strong PS fluorescence. We could no longer use temporal filtering. We have observed that the singlet oxygen luminescence intensity is less than 5% of the intensity of the PS fluorescence at 1.27 μm. Thus, it is crucial to have high signal collection efficiency and low detector noise for an optimized signal-to-noise ratio (SNR). CW spectroscopic detection of singlet O_2 also requires a sufficient number of wavelength data points outside the 1270 nm region to measure the PS fluorescence as illustrated in Figure 12 above. For the weak signals in tissue, the three filter approach was inadequate to discriminate the singlet O_2 luminescence from the PS fluorescence for a cw light. To assess whether we could extract singlet oxygen signals from the dominating PS emission, we designed, built, and tested two systems shown in Figure 15.

We increased the number of narrow bandpass filters from three to nine to provide more data points in the spectral region of the singlet O_2 luminescence (Figure 15a). Figure 16 shows data obtained by this approach from an *in vitro* sample of the benzoporphyrin derivative (BPD) photosensitizer dissolved in oxygen saturated methanol. Using this filter wheel approach, we completed an animal study at Dartmouth and were able to monitor the singlet oxygen produced during PDT with cw laser excitation of tumors in mice.[44] However, for several mice, even nine filters were inadequate to discriminate the singlet oxygen signals from the background PS.

This approach also had a signal collection bandwidth limitation. A filter wheel and a single element, nonpixelated detector forces the spectral information to be measured sequentially, i.e., the spectrum is spread in time (Figure 15a). For each filter, only the transmitted photons are detected, discarding all other out-of-band wavelength components. In this case, the measurement duty cycle or signal detection efficiency is low, which can be described as $\delta\lambda/\Delta\Lambda$, where $\delta\lambda$ is the bandwidth of the filters, and $\Delta\Lambda$ is the entire spectral range to be measured. In a sense, the filter wheel is a “boxcar integrator” approach because the spectral points are recorded sequentially. For *in vivo* studies, it is crucial to minimize the singlet oxygen measurement time to reduce systematic errors due to animal movements such as

breathing. To address this issue and to provide more spectral data points, we designed and built a multispectral instrument. Figure 15b illustrates an array detector-based spectrometer, and these are often referred to as optical multichannel analyzers (OMAs). In this case, the wavelengths are spread in space by a diffraction grating. An array sensor (e.g., a 2D camera) measures all the wavelength components simultaneously. At Dartmouth College, we also completed a study[45] with tumor-burdened mice using a 2D cooled InGaAs camera spectrometer illustrated in Figure 15b. Compared to the filter wheel, the SNR was much higher. For cw excitation, the corresponding signal detection efficiency (in time) of the parallel detection is essentially 100%. However, due to the unavoidable “dark noise” and “readout noise”, these array detectors are noisier than cooled single element detectors and much more expensive.

We are now investigating a system that takes advantage of a sensitive, low noise, single element InGaAs detector for simultaneous detection of many wavelengths. This is based on a computational spectroscopy (CS) method[46] integrated into a conventional spectrometer setup. However, instead of using an array detector as shown in Figure 15b, the CS approach uses a spatial-light-modulator (SLM) in the focal plane (where the array detector would normally be placed). We use a digital micro mirror (DMD) that selectively reflects a set of user-defined wavelength components to a focusing lens followed by a single element InGaAs detector. In this case, the detector readout is the integration of multiple wavelength components selected by the DMD. In order to separate the contributions of each individual wavelength, a series of measurements are made, with each time the DMD reflecting a different set of wavelengths. For n spectral components to be measured, n measurements are made to form a complete set that can be described by a set of linear algebraic equations. The spectral information is retrieved by inverting a matrix to produce the intensity at each of the n wavelengths observed. This approach was originally developed by DeVerse et al.[46]

Using this technique, we have completed a preliminary animal study at Cleveland Clinic. The study measured both the PS and $^1O_2$ luminescence produced during PDT treatment using a 405 nm LED light to treat a cohort of eight mice with squamous cell carcinoma (SCC) lesions on their skin. These lesions were induced by UV irradiation over several weeks leading up to the experiments to allow the lesions to grow to diameters of 2–3 mm.[47,48] The results of this preliminary study are summarized in Figure 17.

Figure 17a shows example measurements of PS and $^1O_2$ from a living mouse during the treatment. High SNR measurements of $^1O_2$ were demonstrated by the high-fidelity Gaussian fit (fit goodness $R^2 = 0.98$) to the measurement data points in the $^1O_2$ spectrum (lower panel of Figure 17a). To the best of our knowledge, the spectra in Figure 16a are the first high-resolution PS/$^1O_2$ spectra measured from a living mouse during ALA PDT treatment of skin cancer. Photographs of the mouse and tumors as a function of time pre- and post-treatment are used to record the post-treatment tumor reduction by the PDT treatment, shown in Figure 17b. Visual inspection of the photographs indicates that the treated areas, e.g., within the red circles, clearly show the tumors were shrinking over the two-week period following the one-time PDT treatment. In contrast, untreated tumors (outside the circles) continued to grow. The singlet O_2 measurement was correlated to the tumor reduction rate as shown

in Figure 17c. A linear fit to the data points demonstrates the positive correlation between measured singlet O_2 measurements and the tumor reduction rate. These data demonstrate that we are able to monitor real-time PS and singlet oxygen produced by a cw treatment light source. Although this was for a small cohort of only eight mice, the correlation of tumor regression post treatment is positive. These studies are ongoing. We conclude that this approach provides the best signal-to-noise for singlet O_2 compared to previous *in vivo* studies we have completed using more traditional detection methods.[34,41,44,45,49–51] We plan to complete more extensive animal studies and some human subject studies with the new detection system.

CONCLUSION

We have attempted to describe the rather long and unanticipated journey from fundamental molecular kinetic and spectroscopic investigations of high power gas lasers to current developments in a promising cancer therapy diagnostic. The lessons learned in the early work on reacting gaseous flow-fields were extremely valuable and relevant to studies in tissue. Both have excessive background optical emissions within the relevant spectral range. Both display large stochastic noise fluctuations, and both present challenges of optical collection of the very weak singlet oxygen emission. While the early experience with singlet oxygen detection during the COIL experiments provided valuable technical knowledge, the close industrial-academic medical center collaborations were absolutely essential for the translation of this knowledge to possible clinical applications. Indeed, the fruitful, long-lasting collaborations involving researchers from myriad scientific disciplines led to novel approaches and studies that would have not otherwise been possible.

ACKNOWLEDGMENTS

We gratefully acknowledge several funding agencies for support of various facets of this research. S.J.D. would like to particularly thank the Air Force Office of Scientific Research (AFOSR) for support in developing diagnostics for the COIL laser that led eventually to the PDT application. Drs. Don Ball and Mike Berman were the AFOSR monitors. The initial singlet oxygen detection for PDT applications was funded by the Davison Laser Center, Elliot Hospital, Manchester, NH and by an Air Force SBIR contract from the Air Force Research Laboratory, Kirtland AFB, NM (Contract F29601–97-C-0156). We also gratefully acknowledge the support of NCI through several SBIR Grants: No. 5R44CA096243–03, No. 5R44CA128364–03, and No. 4R44CA250727–02. The authors would also like to acknowledge researchers who were key to the success of these endeavors: Seonkyung Lee (PSI), Kristin Galbally Kinney (PSI), Srivalleesha Mallidi (MGH), and Jason Gunn (Dartmouth). We also thank PSI colleagues Terry Rawlins, Bill Kessler, and David Rosen for numerous helpful discussions.

Biographies

Steven J. Davis is the recently retired chief scientist at Physical Sciences Inc. He received his B.S. and Ph.D. degrees in physics from the University of New Hampshire. From 1973 to 1985 he was a research scientist at the Air Force Research Laboratory (AFRL) at Kirtland AFB in Albuquerque, New Mexico. There, he led numerous programs with a focus on basic research for the development of new chemical lasers. He was also a research advisor for several National Research Council (NRC) postdoctoral fellows and for numerous M.S. and Ph.D. students. He joined Physical Sciences Inc. in 1985 and led a variety of programs: atomic and molecular physics, new laser development, science education for K-12 students, and the development of advanced, optically based diagnostics for photodynamic therapy.

Youbo Zhao is a principal scientist at Physical Sciences Inc. He received his B.S. degree in applied physics from Beijing Institute of Technology, Beijing, China, in 1997 and his Ph.D. in optical engineering from Nankai University, Tianjin, China, in 2007. He was a postdoctoral research associate at the Biophotonics Imaging Laboratory, the University of Illinois at Urbana–Champaign, Urbana, Illinois, USA. His research interests include developing and applying optical imaging and sensing technologies to promote advanced biomedical studies and clinical practice.

Ms. Yu is a research scientist at Physical Sciences Inc. in Andover, Massachusetts. She finished her academic studies in 2019, earning a B.S. and M.S. in Bioengineering from Clemson University. She has worked at Physical Sciences Inc. since 2020 on a wide variety of research projects. At PSI, she has worked on a project developing a photodynamic therapy dosimeter to quantify singlet oxygen production, in collaboration with Cleveland Clinic and Dartmouth College. Her research interests are in developing technology with biological and medical applications.

Dr. Maytin is a physician-scientist in the Dermatology and Biomedical Engineering departments at the Cleveland Clinic, Cleveland, Ohio. As an investigative dermatologist, he specializes in basic science and clinical aspects of photodynamic therapy (PDT) and, over the past 20 years, has conducted extensive laboratory research on amino-levulinate-based PDT mechanisms. He has subsequently translated those findings into human clinical trials on the use of combination approaches to improve PDT treatment outcomes for patients with skin cancer and precancer. His research has been continuously supported by the National Institutes of Health (NIH) since 1995.

Dr. Sanjay Anand is an Assistant Professor of Molecular Medicine in the Cleveland Clinic Lerner College of Medicine and a member of the staff in the Department of Biomedical Engineering and in the Dermatology and Plastic Surgery Institute at Cleveland Clinic, Cleveland, Ohio, U.S.A. He has B.Sc. and M.Sc. degrees in Zoology from Banaras Hindu University, a Ph.D. degree in Zoology from the University of Pune, India, and received training (fellowships) at Pennsylvania State University and the Cleveland Clinic. His research focuses on elucidating the transcriptional control mechanisms of solar carcinogenesis and developing photodynamic therapy for skin precancer and cancer treatment. He is interested in developing new combination approaches to enhance the therapeutic outcome of ALA-PDT by modulating the immune response in preclinical and clinical studies.

Dr. Tayyaba Hasan, Ph.D., is a Professor of Dermatology at the Wellman Center for Photomedicine, Harvard Medical School (HMS) and a Professor of Health Sciences and Technology at Harvard-MIT (HST) with a Ph.D. in physical organic chemistry. Dr. Hasan has published over 300 peer-reviewed articles, has been cited more than 30 000 times, and has over 30 inventions to her name. The winner of many lifetime achievement awards, Dr. Hasan is recognized as a leader in the field of photodynamic therapy (PDT). The focus of her research is a study of photochemical and photobiological sciences and, wherever possible, applying the findings to treatment, therapy monitoring, and diagnosis of disease,

primarily in the areas of cancer and infections. Her research is funded by the National Institutes of Health, the Department of Defense, and industry grants.

Dr. Pogue's work in the area of optical imaging devices to guide cancer therapies has led to the invention of a unique system for imaging radiation dosing with Cherenkov emission and another unique approach to imaging hypoxia during surgical resection. The lab has NIH funding, and translational work led to the cofounding of two start-ups, DoseOptics, and QUEL Imaging, the former of which has commercialized direct visualization of radiation dose delivery to patients. He has published more than 450 peer-reviewed papers and is a Fellow of Optica, SPIE, AIMBE, and the National Academy of Inventors. He is Editor-in-Chief of the *Journal of Biomedical Optics*, SPIE Publications.

REFERENCES

(1). Kasper JVV; Pimentel GC Appl. Phys. Lett. 1964, 5, 231.

(2). Derwent RG; Kearns DR; Thrust BA The excitation of iodine by singlet molecular oxygen. Chem. Phys. Lett. 1970, 6 (2), 115.

(3). Derwent RG; Thrush BA Measurements of $O_2(^1\Delta)$ and $O_2(^1\Sigma)$ in discharge flow systems. Trans. Faraday Soc. 1971, 67, 2036.

(4). Derwent RG; Thrush BA The radiative lifetime of the metastable iodine atom $I(5^2P_{1/2})$. Chem. Phys. Lett. 1971, 9 (6), 591.

(5). Derwent RG; Thrush BA Excitation of iodine by singlet molecular oxygen part 1 - mechanism of the I_2 chemiluminescence. Journal of the Chemical Society, Faraday Discussions II 1972, 68, 720.

(6). Derwent RG; Thrush BA Excitation of iodine by singlet molecular oxygen part 2 - kinetics of the excitation of the iodine atoms. Chemical Soc. Faraday Discussions 1972, 53, 162.

(7). McDermott WE; Pchelkin D; Benard DJ; Bousek RR An electronic transition chemical laser. Appl. Phys. Lett. 1978, 32, 469.

(8). Held AM; Halko DJ; Hurst JK Mechanisms of chlorine oxidation of hydrogen peroxide. J. Am. Chem. Soc. 1978, 100 (18), 5732.

(9). Lilenfeld HV; Carr PAG; Hovis FE J. Chem. Phys. 1984, 81, 5730.

(10). Van Benthem MH; Davis SJ J. Phys. Chem. 1986, 90, 902.

(11). Perram GP Int. J. Chem. Kinet. 1995, 27, 817.

(12). Barmashenko BD; Rosenwaks S AIAA J. 1996, 34, 2569.

(13). Heidner RF III; Gardner CE; Segal GI; El-Sayed TM J. Phys. Chem. 1983, 87, 2348.

(14). Carroll DL; Verdeyen JT; King DM; Zimmerman JW; Laystrom JK; Woodard BS; Richardson N; Kittell K; Kushner MJ; Solomon WC Appl. Phys. Lett. 2004, 85 (8), 1320.

(15). Carroll DL; Verdeyen JT; King DM; Zimmerman JW; Laystrom JK; Woodard BS; Benavides GF; Kittell K; Solomon WC XV International Symposium on Gas Flow and Chemical Lasers and High Power Laser Conference, Prague, 2004; SPIE, 2005; p 5777.

(16). Carroll DL; Verdeyen JT; King DM; Zimmerman JW; Laystrom JK; Woodard BS; Benavides GF; Kittell KW; Solomon WC Path to the measurement of positive gain on the 1315-nm transition of atomic iodine pumped by $O_2(a^1\Delta)$ produced in an electric discharge. IEEE J. Quantum Electron. 2005, 41 (2), 213.

(17). Carroll DL; Verdeyen JT; King DM; Zimmerman JW; Laystrom JK; Woodard BS; Benavides GF; Kittell K; Stafford DS; Kushner MJ; Solomon WC Continuous-wave laser oscillation on the 1315 nm transition of atomic iodine pumped by $O_2(a^1\Delta)$ produced in an electric discharge. Appl. Phys. Lett. 2005, 86, 111104.

(18). Rawlins WT; Lee S; Kessler WJ; Davis SJ Observations of gain on the $I(^2P_{1/2} \rightarrow {}^2P_{3/2})$ transition by energy transfer from $O_2(a^1\Delta g)$ generated by a microwave discharge in a subsonic flow reactor. Appl. Phys. Lett. 2005, 86 (5), 051105.

(19). Truesdell KA; Helms CA; Hager GD History of chemical oxygen-iodine laser (COIL) development in the USA. Proceedings of SPIE 2502, Gas Flow and Chemical Lasers: Tenth International Symposium, March 31, 1995.

(20). Masamori E; Walter RF Gas Lasers; CRC Press, Taylor and Francis Group: Boca Raton, FL, 2007.

(21). Raab Ueber O die Wirkung fluorizierender Stoffe auf Infusorien. Z. Biol. 1900, 39, 524–546.

(22). Kautsky H; de Bruijn H Naturwissenschaften 1931, 19, 1043.

(23). Wieshaupt KR; Gomer CJ; Dougherty TJ Identification of singlet oxygen as the cytoxic agent in photo-inactivation of a murine tumor. Cancer Res. 1976, 36, 2326. [PubMed: 1277137]

(24). Kessel D; Castelli M; Reiners J On the Mechanism of PDT-induced Mitochondrial Photodamage. Proceedings of SPIE 2001, 4248, 157.

(25). Fingar VH; Wieman TJ; Wichle SA; Cerrito PB The role of microvascular damage in photodynamic therapy, the effect of treatment on vessel constriction, permeability, and leukocyte adhesion. Cancer Res. 1992, 52, 4914–4921. [PubMed: 1387584]

(26). Lee S; Zhu L; Minhaj AM; Hinds MF; Vu DH; Rosen DI; Davis SJ; Hasan T Pulsed Diode Laser-Based Monitor for Singlet Molecular Oxygen. J. Biomed. Opt. 2008, 13 (3), No. 034010. [PubMed: 18601555]

(27). Dougherty TJ; Gomer CJ; Henderson BW; Jori G; Kessel D; Korbelik M; Moan J; Peng J Photodynamic Therapy. J. of the Nat. Cancer Inst. 1998, 90, 889.

(28). Ochsner M Photophysical and photobiological processes in the photodynamic therapy of tumors. J. of Photochemistry and Photobiology B: Bio. 1997, 39, 1.

(29). Goodell TT; Jacques SL; Gregory KW Evaluating Clinical Outcomes of PDT. Proceedings of SPIE 2001, 4248, 1.

(30). Dougherty TJ Optical Methods for Tumor Treatment and Detection: Mechanisms and Techniques in Photodynamic Therapy X. Progress in Biomedical Optics and Imaging. Proceedings of SPIE 2001, 4248, I–IX.

(31). Kim MM; Penjweini R; Zhu TC Evaluation of singlet oxygen explicit dosimetry for predicting treatment outcomes of benzoporphyrin derivative monoacid ring A-mediated photodynamic therapy. J. Biomed. Opt. 2017, 22 (2), No. 028002. [PubMed: 28301655]

(32). Kim MM; Penjweini R; Gemmell NR; Veilleux I; McCarthy A; Buller G; Zhu TC A feasibility study of singlet oxygen explicit dosmietry (SOED) of PDT by intercomparison with a singlet oxygen luminescence dosimetry (SOLD) system. In Optical Methods for Tumor Treatment and Detection: Mechanisms and Techniques in Photodynamic Therapy XXV; International Society for Optics and Photonics, 2016; vol 9694, p 969406.

(33). Li B; Lin L; Lin H; Wilson BC Photosensitized singlet oxygen generation and detection: Recent advances and future perspectives in cancer photodynamic therapy. Journal of biophotonics 2016, 9 (11–12), 1314–1325. [PubMed: 27136270]

(34). Lee S; Vu DH; Hinds MF; Liang A; Hasan T; Davis SJ Pulsed Diode Laser-Based Singlet Oxygen Monitor for Photodynamic Therapy: in-vivo Studies of Tumor Laden Rats. J. Biomed. Opt. 2008, 13 (6), No. 064035. [PubMed: 19123681]

(35). Parker JG Optical Monitoring of Singlet Oxygen during Photodynamic Treatment of Tumors. IEEE Circuits and Devices Magazine 1987, 3, 10.

(36). Patterson MS; Madsen SJ; Wilson BG Experimental Tests of the Feasibility of Singlet Oxygen Luminescence Monitoring in vivo During Photodynamic Therapy. J. Photochemistry and Photobiology B: Biology 1990, 5, 69.

(37). Niedre MJ; Patterson MS; Boruvka N; Wilson BC Measurement of Singlet Oxygen Luminescence form AML5 Cells Sensitized with ALA-Induced PpIX in Suspension During Photodynamic Therapy and Correlation with Cell Viability After Treatment. Proc. SPIE 2002, 4612.

(38). Niedre M; Patterson MS; Wilson BC Direct Near-Infrared Luminescence Detection of Singlet Oxygen Generated by Photodynamic therapy in Cells In Vitro and Tissues in Vivo. Am. Soc. for Photobiology 2002, 75, 382.

(39). Schmidt R; Afshari E Collisional Deactivation of $O_2{}^1\Delta$ by Solvent Molecules. Ber. Bunsenges. Phys. Chem. 1992, 96, 788.

(40). Egorov SY; Kamalov VF; Koroteev NI; Krasnovsky AA; Toleutaev BN; Zinukov SV Rise and Decay Kinetics of Photosensitized Singlet Oxygen Luminescence in Water. Measurements with Nanosecond, Time Correlated Single Photon Counting Technique. Chem. Phys. Lett. 1989, 163, 421.

(41). Lee S; Isabelle ME; Gabally-Kinney KL; Pogue BW; Davis SJ Dual-channel imaging system for singlet oxygen and photosensitizer for PDT. Biomed. Opt. Express 2011, 2 (5), 1233–1242. [PubMed: 21559134]

(42). Niedre MJ; Yu CS; Patterson MS; Wilson BC Singlet Oxygen Luminescence as an in-vivo photodynamic therapy dose metric: validation in normal mouse skin with topical amino-luvulinic acid. Br. J. Cancer 2005, 92, 298. [PubMed: 15655542]

(43). Niedre MJ; Second AJ; Patterson MS; Wilson BC *In Vitro* Tests of the Validity of Singlet Oxygen Luminescence Measurements as a Dose Metric in Photodynamic Therapy. Cancer Res. 2003, 63, 7986. [PubMed: 14633731]

(44). Moritz TJ; Zhao Y; Hinds MF; Gunn JR; Shell JR; Pogue BW; Davis SJ Multispectral singlet oxygen and photosensitizer luminescence dosimeter for continuous photodynamic therapy dose assessment during treatment. J. of Biomed. Opt. 2020, 25 (6), No. 063810. [PubMed: 32170859]

(45). Zhao Y; Moritz T; Hinds MF; Gunn JR; Shell JR; Pogue BW; Davis SJ High optical-throughput spectroscopic singlet oxygen and photosensitizer luminescence dosimeter for monitoring of photodynamic therapy. Journal of Biophotonics. 2021, 14 (11), No. 00088.

(46). DeVerse RA; Hammaker RM; Fateley WG Realization of the Hadamard multiplex advantage using a programmable optical mask in a dispersive flat-field near-infrared spectrometer. Appl. Spectrosc. 2000, 54 (12), 1751–1758.

(47). Anand S; Rollakanti KR; Horst RL; Hasan T; Maytin EV Combination of oral vitamin D3 with photodynamic therapy enhances tumor cell death in a murine model of cutaneous squamous cell carcinoma. Photochem. Photobiol. 2014, 90 (5), 1126–1135. [PubMed: 24807677]

(48). Rollakanti K; Anand S; Davis SC; Pogue BW; Maytin EV Noninvasive optical imaging of UV-induced squamous cell carcinoma in murine skin: Studies of early tumor development and Vitamin D enhancement of protoporphyrin IX production. Photochem. Phototobiol 2015, 91 (6), 1469–78.

(49). Davis SJ; Rosen DI; Sivimani RK; Burney W Instrument for measurement of singlet oxygen for studies of skin under UVA irradiation. SPIE Photonics West, San Francisco, CA, February 2–7, 2019; SPIE Paper No. 10851–18.

(50). Laubach HJ; Chang SK; Lee S; Rizvi I; Zurakowski D; Davis SJ; Taylor CR; Hasan T In vivo singlet oxygen dosimetry of clinical 5-aminolevulenic acid photodynamic therapy. J. Biomed. Opt. 2008, 13, No. 050504. [PubMed: 19021376]

(51). Mallidi S; Anbil S; Lee S; Manstein D; Elrington S; Kositratna G; Schoenfeld D; Pogue B; Davis SJ; Hasan T Photosensitizer fluorescence and singlet oxygen luminescence as dosimetric predictors of topical 5-aminolevulinic acid photodynamic therapy induced clinical erythema. J. Biomed. Opt. 2014, 19 (2), No. 028001. [PubMed: 24503639]

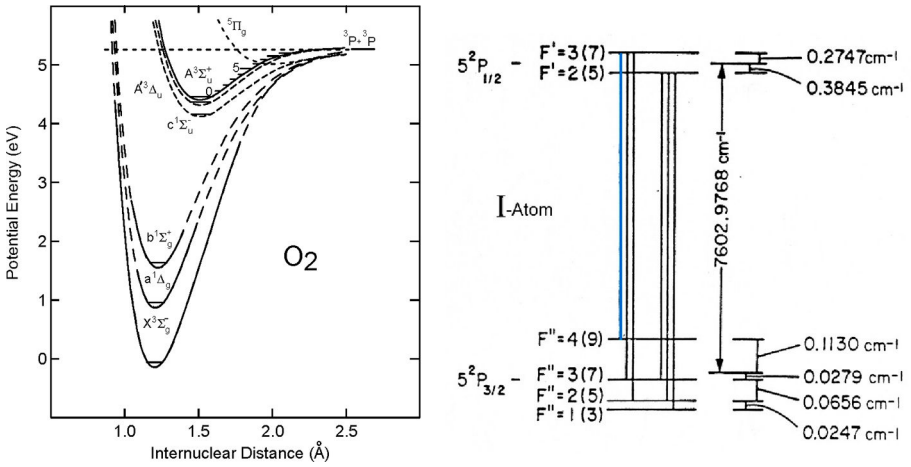

Figure 1.
Energy level diagrams for COIL: (a) molecular oxygen and (b) atomic iodine.

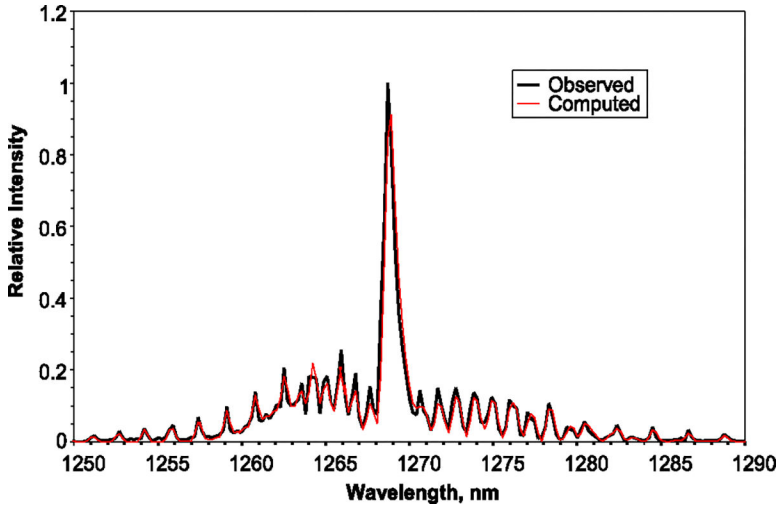

Figure 2.

Rotationally resolved $O_2(a^1\Delta_g \rightarrow X^3\sum_g)$ emission from an electrically excited flow of oxygen and argon.

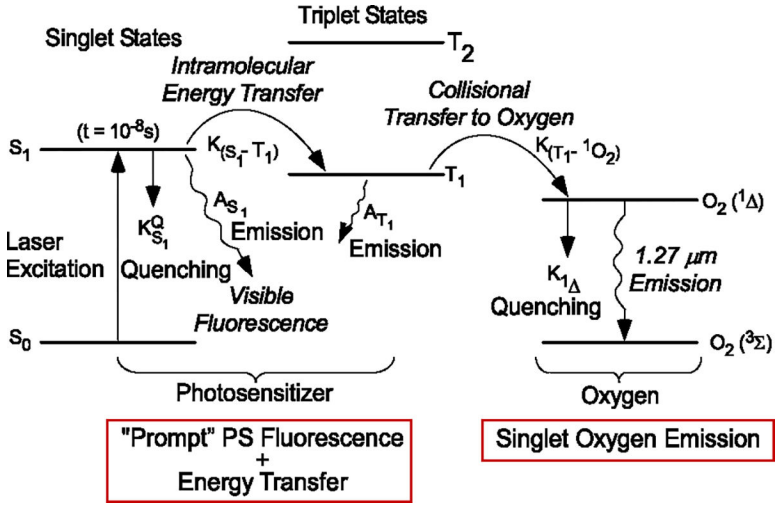

Figure 3.

Mechanism for the production of singlet O_2 in PDT. Reprinted with permission from ref 26. Copyright SPIE 2008.

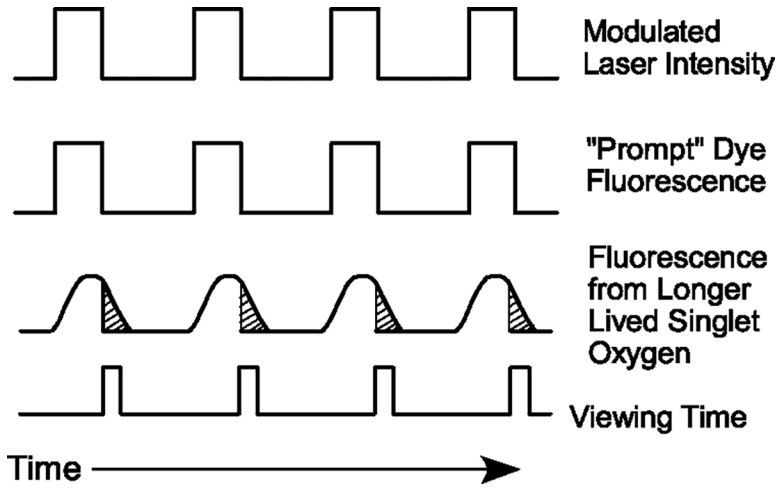

Figure 4.

Singlet O_2 detection strategy using a pulsed diode laser for PS excitation. Reprinted with permission from ref 26. Copyright SPIE 2008.

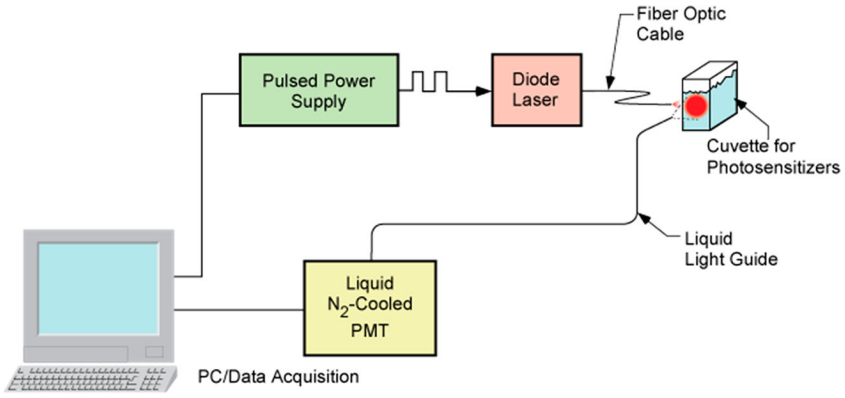

Figure 5.
Apparatus for initial *in vitro* measurements of PS and singlet O_2 optical emissions.

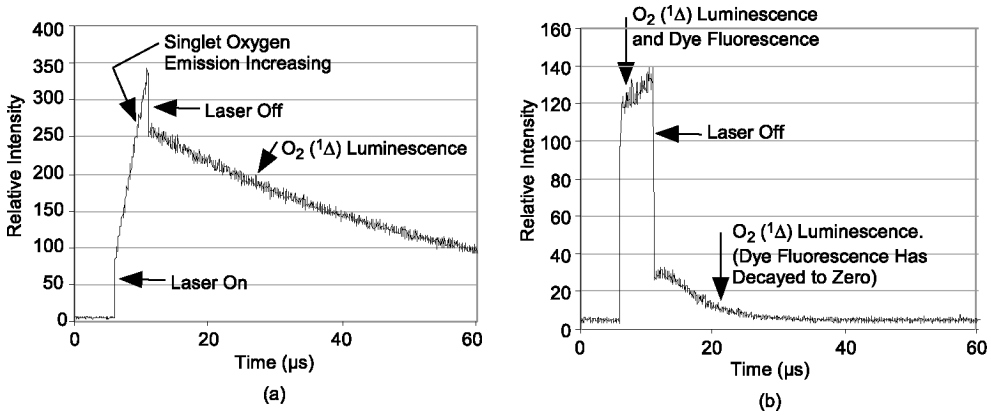

Figure 6.

Temporal evolution of the IR emission centered at 1.27 μm following 5 μs excitation of Cl-e6: (a) acetone, (b) water. Reprinted with permission from ref 26. Copyright SPIE 2008.

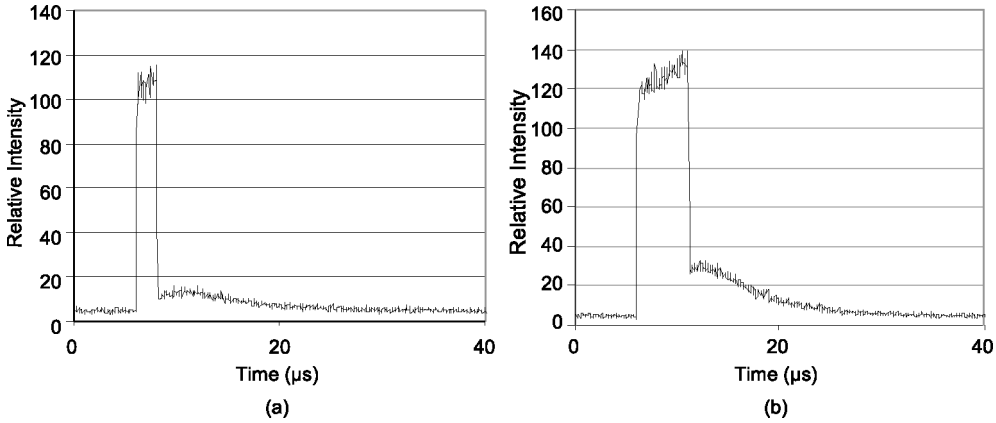

Figure 7.

Comparison of the observed signal at 1.27 μm produced in Cl-e6 with two diode laser excitation pulse widths. (a) $\tau_p = 2$ μs, (b) $\tau_p = 5$ μs. Reprinted with permission from ref 26. Copyright SPIE 2008.

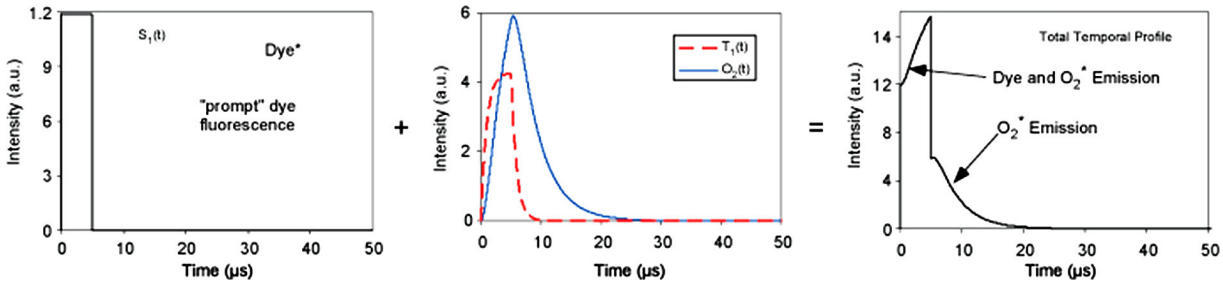

Figure 8.

Model predictions showing components of the PDT process for long pulse (5 μs) diode laser excitation. Reprinted with permission from ref 26. Copyright SPIE 2008.

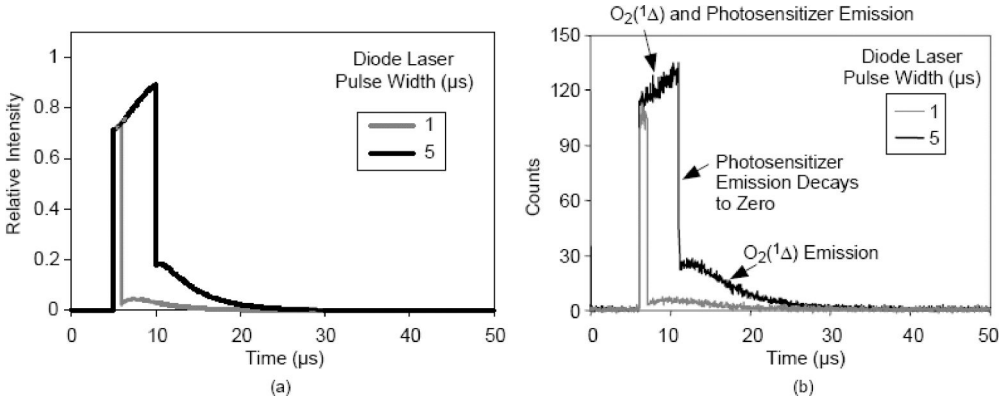

Figure 9.

Temporal profiles for the radiative emission from singlet oxygen in water with different laser pulse widths: (a) prediction using our kinetic model with $\tau_T = 1\ \mu s$, $\tau^1\Delta = 4\ \mu s$, $\phi_T = 0.4$ and $\phi_\Delta = 0.7$ (b) experimental results with Cl-e6 in aqueous solution. Reprinted with permission from ref 26. Copyright SPIE 2008.

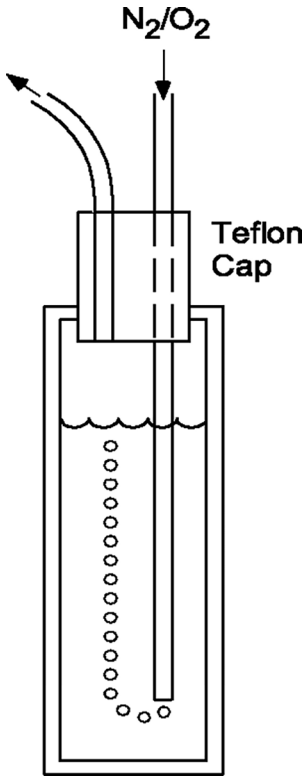

Figure 10.
Method for controlling the concentration of oxygen dissolved in the solution in the cuvette.

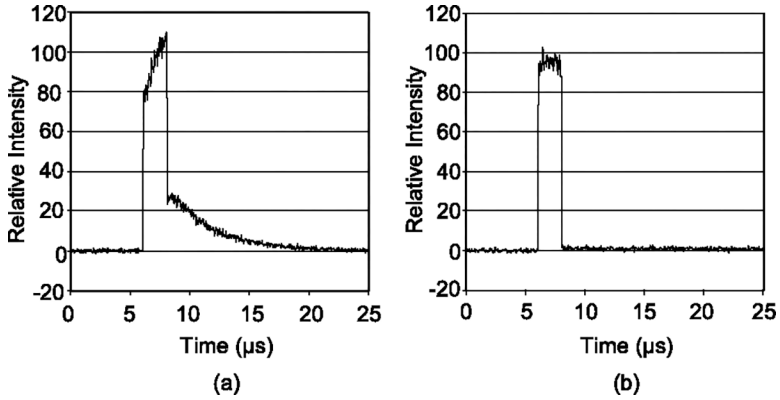

Figure 11.

Comparison of SWIR emission observed in Cl-e6 in water using a 2 μs diode laser pulse. (a) Oxygenated sample and (b) same sample deoxygenated. Reprinted with permission from ref 26. Copyright SPIE 2008.

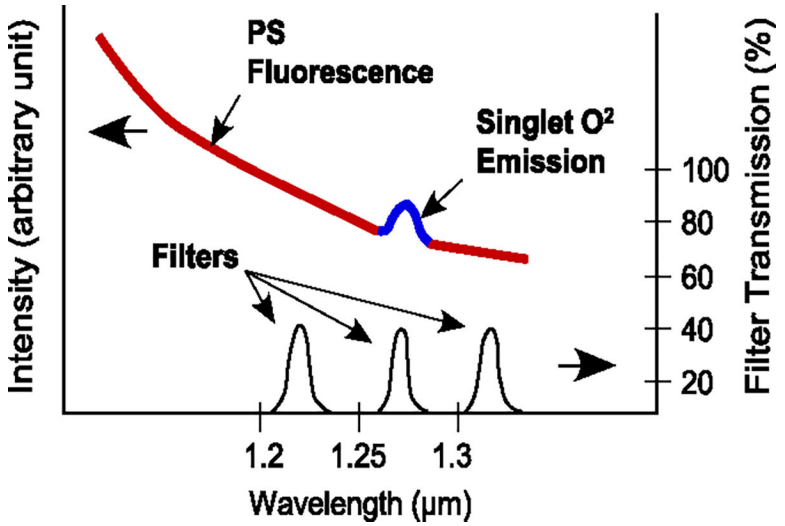

Figure 12.

Typical spectra for PS fluorescence and singlet oxygen emission. The transmission curves of the three filters are also illustrated. Reprinted with permission from ref 34. Copyright SPIE 2008.

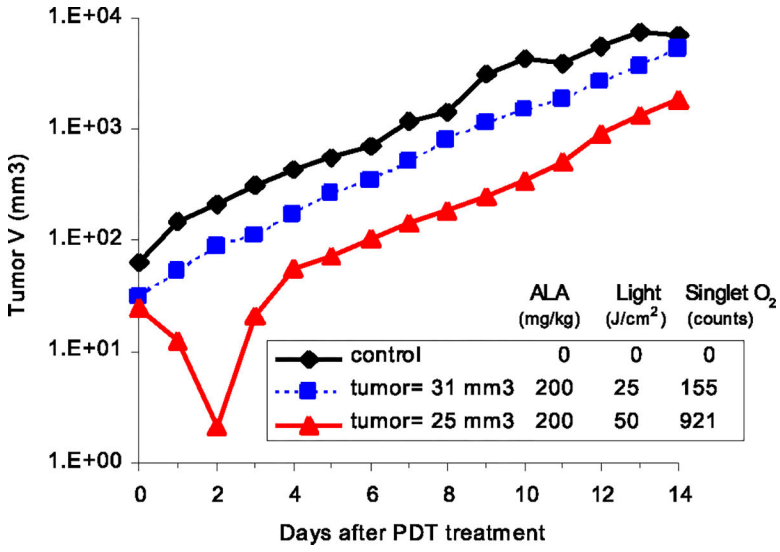

Figure 13.

Tumor regression data for three rats including one control. Reprinted with permission from ref 34. Copyright SPIE 2008.

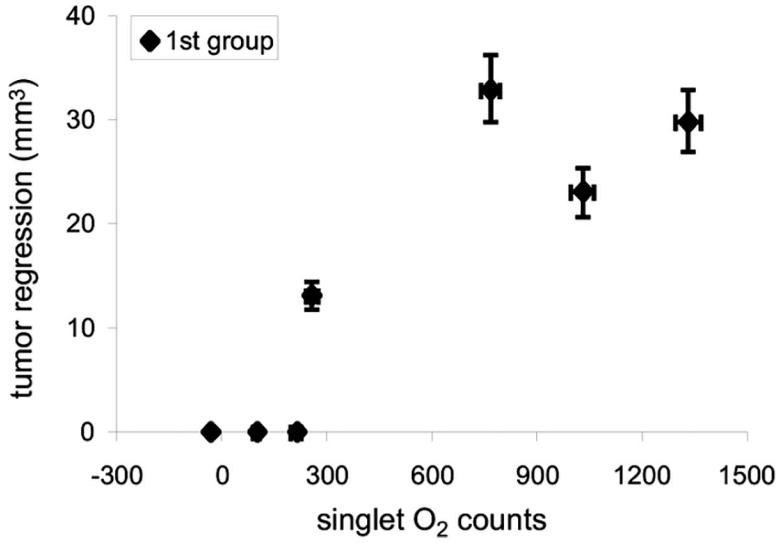

Figure 14.

Measured tumor regression as a function of singlet oxygen counts for a cohort of seven rats. Reprinted with permission from ref 34. Copyright SPIE 2008.

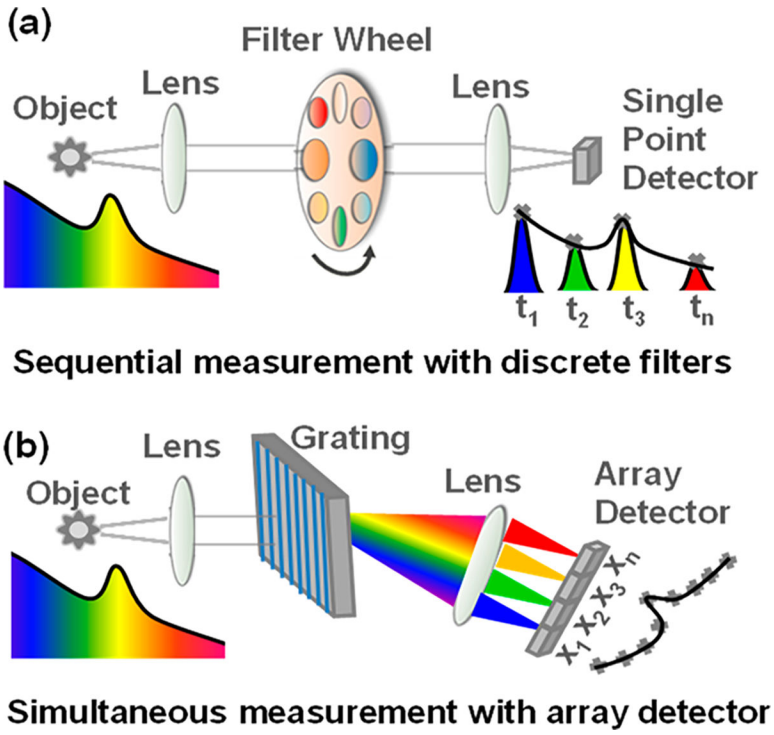

Figure 15.
Schematic illustration of two spectroscopy approaches: (a) filter wheel with a single element detector and (b) a 2-D array detection system.

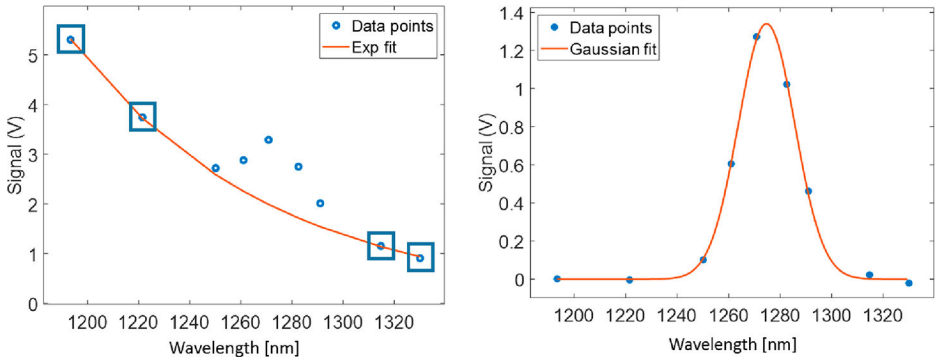

Figure 16.

Method to extract a singlet oxygen signal: (a) Determination of photosensitizer (benzoporphyrin derivative: BPD) fluorescence background based on exponential fitting (red curve) to the four out of band spectral data points indicated by the blue squares. (b) Gaussian fitting (red curve) to the PS fluororescence background subracted data points (blue dots), which depicts the extracted singlet oxygen ($^1O_2$) signal. Reprinted with permission from ref 44. Copyright SPIE 2020.

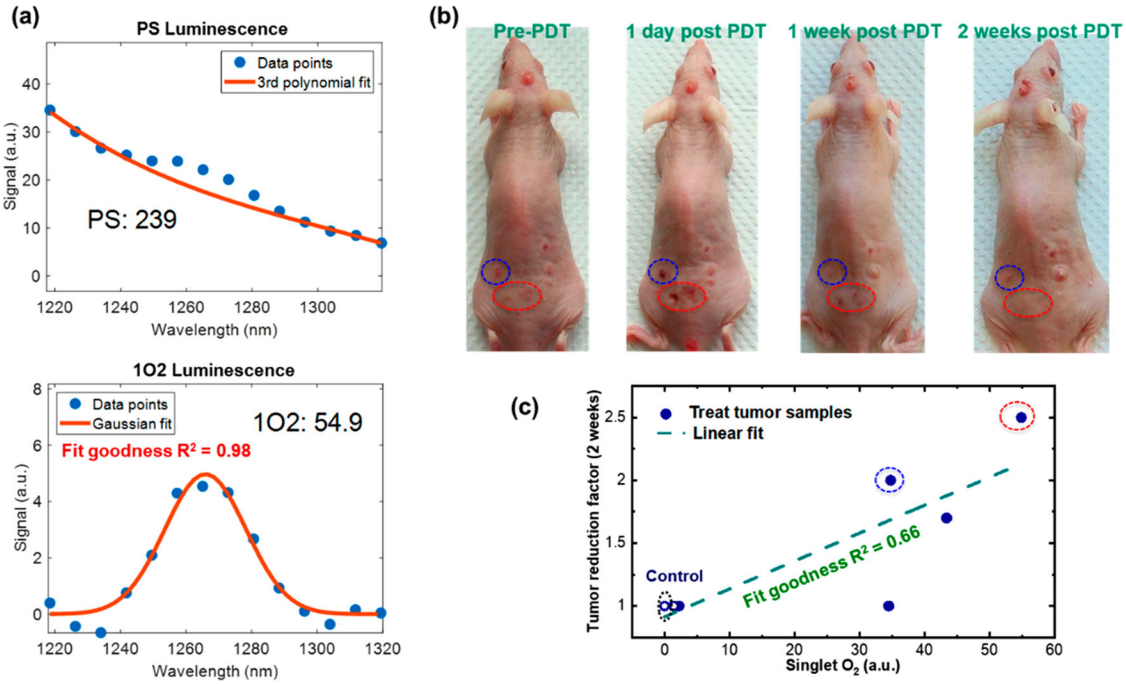

Figure 17.

Summary of $^1O_2$ measurements during *in vivo* ALA PDT treatment performed at Cleveland Clinic. (a) Recorded spectra for PS (top) and $^1O_2$ (bottom) for a living mouse (shown in b). (b) Photographs of the mouse showing tumor regression in PDT treated areas (circled) at days 1, 7, and 14 subsequent to treatment. (c) Correlation of tumor regression as a function of $^1O_2$ measured during treatment. The circled data points correspond to the tumor lesions in b.

Table 1.

Photosensitizers Used in the Study

photosensitizer	molecular weight (g/mol)
aluminum phthalocyanine tetrasulfonate (AlP_cS4)	895.2
chlorin e6 (Cl-e6)	594.6
meso-tetra-(4-sulphonatophenyl)-porphine-dihydrochloride (T4PS-4)	1007.7
hematoporphyrin derivative (HPD)IX (limited studies)	598.7

Table 2.

Summary of Measurements[a]

		$O_2(^1\Delta)$ lifetime	PS triplet state lifetime
dye	**solvent**	**τ_Δ (μs)**	**τ_T (μs)**
Cl-e6	acetone	49.5	0.4
	methanol	9.4	0.5
	water	3.7	0.9
	water with 5% FBS	0.4	5.0
T4SP	methanol	9.7	0.7
	water	4.4	2.7
AlP_cS4	methanol	10.6	0.6
	water	4.3	2.0

[a]Note: Literature values of τ_Δ in acetone, methanol, and water are 51 μs, 9.5 μs, and 4.2 μs, respectively (refs 35–40)